Izvestiya, Atmospheric and Oceanic Physics, Vol. 40, No. 3, 2004, pp. 276–290. Translated from Izvestiya AN. Fizika Atmosfery i Okeana, Vol. 40, No. 3, 2004, pp. 314–329.

Spherical Radiative Transfer Model with Computation of Layer Air Mass Factors and Some of Its Applications

O. V. Postylyakov

Oboukhov Institute of Atmospheric Physics, Russian Academy of Sciences, Pyzhevskii per. 3, Moscow, 119017 Russia

e-mail: ovp@ifaran.ru; Web: http://postylyakov.narod.ru

Received January 8, 2003; in final form, January 6, 2004

Abstract—A radiative transfer model was designed for use in inverse problems of atmospheric optics. The model calculates intensities and their derivatives with respect to absorption. In other notations, these derivatives are known as weighting functions or layer air mass factors. Multiple scattering radiation in the model is evaluated by the Monte Carlo method. Radiative transfer is simulated for a spherical shell atmosphere taking into account polarization, Rayleigh and aerosol scattering, gas and aerosol absorption, and Lambert surface albedo. The speed of intensity computations accurate to 1% is approximately the same as in other authors' pseudospherical models used for comparison. The time required for simultaneous computation of intensities and their derivatives is only 1.2–1.8 times as much as the time required for the computation of intensities alone. The model was compared with other spherical and pseudospherical models for geometries in which the sphericity of the atmosphere is important: twilight observations from the ground and limb scatter observations from space. The layer air mass factors calculated by different models were also compared. The influence of approximate (single scattering) computation of weighting functions on the accuracy of ozone profile retrievals was investigated for the Umkehr method used as an example. It was shown that the single scattering approximation gives additional large retrieval errors.

INTRODUCTION

Passive remote sensing in the UV and visible spectral ranges is used to determine the gas composition and aerosol characteristics of the atmosphere from the ground, satellites, and aircraft. Remote sensing based on simpler schemes (such as ozone, nitrogen dioxide, and aerosol retrieval from direct sunlight measurements with ground-based ([1–7], etc.) and satellite photometers (SAM, SAGE, SAGE II [8], SMF-2 [9]), zenith sky observations for ozone content determination ([1, 10, 11], etc.), nadir sounding of ozone from satellites (the instruments TOMS, SBUV, SBUV/2 [12], BUFS [13])) have promoted the development of more advanced measurement models and have provided a better understanding of the approaches to the solution of inverse problems. On the one hand, this resulted in the transition from multiwave to spectral sounding techniques for the atmosphere (Ozone-M/Mir [14], GOME, [15], and subsequent instruments), which made it possible to increase the number of observed gases due to routine or occasional measurements of O_2, O_4, NO, NO_3, OClO, ClO, BrO, IO, HCHO, SO_2, H_2O, HNO_3, HO_2, and $ClONO_2$ contents. On the other hand, limb-viewing geometry (more difficult to interpret) has been used as a major or additional observation geometry (the instruments OSIRIS [16], SAGE III [17], SCIAMACHY [18], GOMOS [19], OMPS [20]). This allows one to increase the coverage of satellite measurements, while preserving the high high-altitude resolution typical of direct sunlight observations, and subsequently pass to solving two- and three-dimensional tomography problems. In ground-based optical sounding, the interest of researchers has also shifted toward spectral techniques and more informative geometry—twilight observations. Twilight measurements make it possible to enhance the sensitivity of optical sounding and, in some cases, to determine not only the total content but also the vertical distribution of atmospheric constituents ([21–25], etc.).

The model of optical measurements is based on the theory of radiation transfer in the atmosphere. The problem of simulating spectral measurements required the development of efficient methods for calculating scattered radiation for large arrays of slightly differing wavelengths. In most cases, this is associated with bulky computations for small variations in the parameters of the atmospheric state, which can be effectively implemented through the calculation of radiative transfer characteristics for a single wavelength—the linearization point for the radiative transfer equation—and the derivatives of these characteristics with respect to a varying parameter of the atmospheric state. The radia-

tive transfer characteristics and, simultaneously, their derivatives with respect to optical parameters are also required for solving inverse problems in atmospheric optics. The derivatives calculated are used to linearize the transfer operator, followed by the consideration of a linear measurement scheme, or they are used in iterative algorithms for solving an inverse problem. For this reason, a radiative transfer model designed for remote sensing must not only compute the radiative transfer characteristics but also involve an efficient algorithm for computing their derivatives with respect to the parameters of the atmospheric state. An accurate interpretation of the most informative limb scattered and twilight measurements must be based on a model with a spherical atmosphere.

In the foreign literature dealing with inverse problems in atmospheric optics, the derivatives with respect to optical characteristics are frequently referred to as weighting functions, following Rodgers' terminology [26]. We also consider the concept of the effective air mass factor of an atmospheric layer, which is related to the derivative. Introduced for scattered radiation, the concept of the effective air mass factor of a layer has an illustrative physical meaning similar to its counterpart for direct radiation.

A general approach to the design of radiative transfer models with computation of weighting functions is based on perturbation theory and was first proposed in [27]. The evaluation of derivatives by the Monte Carlo method was originated in [28]. The first efficient algorithm for calculating weighting functions for radiation transfer was first designed for the model described in [29]. That algorithm was implemented in spherical geometry for computing the derivatives with respect to the aerosol scattering factor in double local Monte Carlo estimation. The idea of [29] on the computation of derivatives was further developed in [57]. Other models with computation of weighting functions have been developed in recent years: the GOMETRAN finite-difference model [30], the LIDORT discrete ordinate model [31], the LIRA Gauss–Seidel iteration model [32], and the CDI model based on a combined integro-differential approach [33; A. Rozanov, personal communication]. These models do not take into account polarization and were designed for a plane-parallel atmosphere, but, as a rule, they have pseudospherical modifications. In pseudospherical models, only single scattering is treated in spherical geometry, while scattering of a higher order is treated for a plane-parallel atmosphere. Some questions related to the linearization of the transfer equation with respect to aerosol characteristics with allowance for multiple scattering were also considered in [34–36].

A radiative transfer model designed for use in inverse problems of atmospheric optics is presented in this paper. The principles of the model construction are described, and the results of its comparison with other radiative transfer models are briefly outlined. The possibility of improving retrieval results by replacing weighting functions computed in the single scattering approximation with weighting functions taking into account multiple scattering is considered.

METHOD FOR CALCULATING DERIVATIVES, WEIGHTING FUNCTIONS, AND LAYER AIR MASS FACTORS

The application of the Monte Carlo method to atmospheric optics is based on the fact that light propagation can be treated as a random Markov chain of collisions between photons and atmospheric molecules, which result in either scattering or absorption of photons. The Monte Carlo method simulates random paths of this chain on a computer and calculates its characteristics, which are estimates of the desired quantities [29, 37–39]. Importantly, a probability estimate of the accuracy of the results obtained can be simultaneously calculated in Monte Carlo simulation. Specialized simulation techniques have been developed to minimize CPU time for various observation conditions. These techniques use modified algorithms simulating photon passage through the atmosphere and take into account the symmetry of problems.

Let us consider the theoretical substantiation of the method for calculating derivatives used in the model under consideration. Light propagation through the atmosphere is described by an integral transfer equation for the photon collision density $\rho = \rho(\mathbf{x})$ in the phase space X:

$$\rho = \mathbf{K}\rho + \psi, \tag{1}$$

where $\psi = \psi(\mathbf{x})$ is the density of initial collisions, $\mathbf{x} = (r, \omega) \in X$, r is the radius vector of a point, ω is a unit direction vector, and $\mathbf{K}$ is an integral operator whose kernel $k(\mathbf{x}', \mathbf{x})$ is the transition density of a photon from $\mathbf{x}'$ to $\mathbf{x}$:

$$\int_X k(\mathbf{x}', \mathbf{x})d\mathbf{x} = \frac{\sigma_S(r')}{\sigma(r')} \le 1.$$

When the photon does not reach the Earth's surface, the kernel is given by

$$K(\mathbf{x}', \mathbf{x}) = \frac{\sigma_S(r')}{\sigma(r')}\frac{g(\mu, r')e^{-\tau(r', r)}\sigma(r)}{2\pi\|r - r'\|^2}\delta(\omega - s),$$
$$\mu = (s, \omega'), \quad s = \frac{1}{\|r - r'\|}(r - r'), \tag{2}$$

where $\sigma_S(r)$ is the scattering cross section of the atmosphere at r, $\sigma(r)$ is the total cross section for the interaction of a photon with the atmosphere, $g(\mu, r)$ is the scattering phase function normalized to unity, $\delta(y)$ is the delta function, and $\tau(r', r) = \int_0^{\|r-r'\|} \sigma(r' + ls)dl$ is the optical length of $[r', r]$. If a photon falls on the Earth's surface, the kernel $k(\mathbf{x}', \mathbf{x})$ takes into account the reflecting properties of the surface. The initial collision density $\boldsymbol{\psi}(\mathbf{x})$ is a function of the source density $\mathbf{s}(\mathbf{x}')$: $\boldsymbol{\psi} = \mathbf{K}\mathbf{s}$, where the integral operator $\mathbf{K}$ has the kernel $k(\mathbf{x}', \mathbf{x}) = \frac{e^{-\tau(r', r)}\sigma(r)}{\|r - r'\|^2}\delta(\omega' - s)\delta(\omega - s)$.

The collision density $\rho(\mathbf{x})$ is related to the solution of the integro-differential transfer equation [the flux density or intensity $\mathbf{I}(\mathbf{x})$] by the equality $\rho(\mathbf{x}) = \sigma(r)\mathbf{I}(\mathbf{x})$ (if any photon carries unit energy).

In remote sensing of the atmosphere, it suffices to estimate a small set of linear functionals $I_\varphi = \int_X \varphi(\mathbf{x})\rho(\mathbf{x})d\mathbf{x}$ of the total collision density field ρ, where $\rho(\mathbf{x}) \in L_1$ (L_1 is the space of absolutely integrable functions) and $\varphi(\mathbf{x}) \in L_\infty$ (L_∞ is the space of almost everywhere bounded functions) [or $\rho(\mathbf{x}) \in N_1$ (N_1 is the space of generalized densities of measures of bounded variation) and $\varphi(\mathbf{x}) \in C$ (C is the space of continuous bounded functions)]. For example, a signal I_* from a receiver $X_* = S_* \oplus \Omega_*$ of volume S_* and field of view Ω_* can be received by using the function

$$\varphi_*(\mathbf{x}) = \frac{1}{\sigma(r)}\delta_{\Omega_*}(\omega)\delta_{S_*}(r) = \frac{1}{\sigma(r)}\delta_{X_*}(\mathbf{x}),$$

where $\delta_{\Omega_*}(\omega) = 1$ for $\omega \in \Omega_*$, $\delta_{\Omega_*}(\omega) = 0$ for $\omega \notin \Omega_*$, $\delta_{S_*}(r) = 1$ for $r \in S_*$, and $\delta_{S_*}(r) = 0$ for $r \notin S_*$ are the indicator functions of Ω_* and S_*, respectively; and $\delta_{X_*}(\mathbf{x}) = \delta_{\Omega_*}(\omega)\,\delta_{S_*}(r)$. Indeed, for I_* we have

$$I_* \equiv \int_{S_*}\int_{\Omega_*} \mathbf{I}(r, \omega)d\omega dr = \int_{S_*}\frac{1}{\sigma(r)}\int_{\Omega_*}\rho(r, \omega)d\omega dr = I_\varphi|_{\varphi = \varphi_*}. \quad (3)$$

When I_φ is estimated by direct Monte Carlo simulation, paths of a photon originating from a source of density $\mathbf{s}(\mathbf{x})$ are picked at random. It is admitted that the photon can escape from the atmosphere or can be absorbed after a random number N of collisions. Consider the case when the source is located outside the atmosphere. The initial photon's position $\zeta_0 \sim \mathbf{s}(\mathbf{x})$ in the phase space and the positions $\zeta_n \in X$ ($n = 1, N$) at which the photon experiences collisions form a homogeneous Markov chain $\zeta_{n-1} \xrightarrow{\mathbf{K}} \zeta_n$. An unbiased estimator ξ: $I_\varphi = E\xi$ of I_φ is the sum $\xi = \sum_{n=1}^N \varphi(\zeta_n)$. We can randomly choose another Markov chain with a transition density $\mathbf{K}'$: $\zeta'_{n-1} \xrightarrow{\mathbf{K}'} \zeta'_n$. In this case, the expression $\xi' = \sum_{n=1}^N Q_n\varphi(\zeta'_n)$ with weights $Q_n = Q_{n-1}\frac{k(\zeta'_{n-1}, \zeta'_n)}{k'(\zeta'_{n-1}, \zeta'_n)}$ and $Q_0 = 1$ is an unbiased estimator $I_\varphi = E\xi'$ of the functional I_φ.

The weighting functions are calculated as follows. Along with the atmosphere with the characteristics given by kernel (2), we consider a perturbed atmosphere in which the absorption cross section is increased by $\Delta\sigma$ in R_+. Its characteristics will be denoted by index +. If $\delta_+(r) = 1$ for $r \in R_+$ and $\delta_+(r) = 0$ for $r \notin R_+$ is the indicator function of the set R_+, then the cross sections for the perturbed atmosphere are $\sigma_+(r) = \sigma(r) + \Delta\sigma \cdot \delta_+(r)$ and $\sigma_{+s}(r) = \sigma_s(r)$.

When I_φ is measured, the weighting function for R_+ is defined as

$$w_\varphi(R_+) \equiv \frac{dI_\varphi}{d\sigma} \equiv \lim_{\Delta\sigma \to 0}\frac{I_{+\varphi} - I_\varphi}{\Delta\sigma}; \quad (4)$$

i.e., $w_\varphi(R_+)$ is the derivative of I_φ with respect to $\sigma(r)$ for $r \in R_+$. The functional $I_{+\varphi}$ for the perturbed atmosphere is estimated from random paths of the Markov chain $\{\zeta_n = (r_n, \omega_n) \in X, n = 0, N\}$ for the unperturbed atmosphere. Denoting by $l_+(r, r')$ the photon's free path in R_+ on the interval $[r, r']$, we find the weights $Q_0 = 1$ and

$$Q_n = Q_{n-1}\frac{k_+(\zeta_{n-1}, \zeta_n)}{k(\zeta_{n-1}, \zeta_n)} = Q_{n-1}\frac{\sigma(r_{n-1})}{\sigma_+(r_{n-1})} \times \frac{e^{-\tau_+(r_{n-1}, r_n)}}{e^{-\tau(r_{n-1}, r_n)}}\frac{\sigma_+(r_n)}{\sigma(r_n)} = Q_{n-1}\frac{\sigma(r_{n-1})}{\sigma(r_{n-1}) + \Delta\sigma\delta_+(r_{n-1})} \times \exp(-l_+(r_{n-1}, r_n)\Delta\sigma)\frac{\sigma(r_n) + \Delta\sigma\delta_+(r_n)}{\sigma(r_n)}$$

$$= Q_{n-1}\left(1 + \frac{\Delta\sigma}{\sigma(r_{n-1})}\delta_+(r_{n-1})\right)^{-1} \times \exp(-l_+(r_{n-1}, r_n)\Delta\sigma)\left(1 + \frac{\Delta\sigma}{\sigma(r_n)}\delta_+(r_n)\right)$$

$$= \exp\left(-\Delta\sigma\sum_{i=1}^n l_+(r_{i-1}, r_i)\right)\left(1 + \frac{\Delta\sigma}{\sigma(r_n)}\delta_+(r_n)\right).$$

The last equality is true because the source (and, hence, the point r_0) lie outside the atmosphere: $\delta_+(r_0) = 0$. The difference between the perturbed $I_{+\varphi}$ and unperturbed I_φ intensities is expressed as

$$I_{+\varphi} - I_\varphi = E\xi_+ - E\xi = E\sum_{n=1}^{N}((Q_n - 1)\varphi(\zeta_n))$$

$$= E\sum_{n=1}^{N}\left\{\varphi(\zeta_n)\left(\exp\left(-\Delta\sigma\sum_{i=1}^{n} l_+(r_{i-1}, r_i)\right)\right.\right.$$

$$\left.\left.\times\left(1 + \frac{\Delta\sigma}{\sigma(r_n)}\delta_+(r_n)\right) - 1\right)\right\} = \Delta\sigma E\sum_{n=1}^{N}\{\varphi(\zeta_n)$$

$$\times\left(-\sum_{i=1}^{n} l_+(r_{i-1}, r_i) + \frac{1}{\sigma(r_n)}\delta_+(r_n)\right)\right\} + o(\Delta\sigma)$$

$$= \Delta\sigma w_\varphi(R_+) + o(\Delta\sigma),$$

which yields the following formula for calculating the weighting functions:

$$w_\varphi(R_+) = \frac{dI_\varphi}{d\sigma}$$

$$= -E\sum_{n=1}^{N}\left\{\varphi(\zeta_n)\left(\sum_{i=1}^{n} l_+(r_{i-1}, r_i) - \frac{1}{\sigma(r_n)}\delta_+(r_n)\right)\right\}. \quad (5)$$

For the signal I_* [see (3)] on a receiver located outside the domain $R_+ : S_* \cap R_+ = \varnothing$, the weighting functions are given by

$$w_*(R_+) = -E\sum_{n=1}^{N}\left\{\frac{1}{\sigma(r_n)}\delta_{X_*}(\zeta_n)\sum_{i=1}^{n} l_+(r_{i-1}, r_i)\right\}. \quad (6)$$

When the atmosphere is symmetrically symmetric or plane-parallel and R_+ is a layer of thickness L_+, it is reasonable to introduce the concept of an effective air mass factor of the layer R_+ for the observed parameter I_φ:

$$m_\varphi(R_+) = \frac{E\sum_{n=1}^{N}\left\{\varphi(\zeta_n)\sum_{i=1}^{n} l_+(r_{i-1}, r_i)\right\}}{L_+E\sum_{n=1}^{N}\varphi(\zeta_n)}. \quad (7)$$

The effective air mass factor of layer R_+ is equal to the mean free path (normalized by L_+ in R_+) of photons reaching the receiver. When the receiver is located outside R_+, the weighting functions are related to the effective layer air mass factor by the equality

$$w_\varphi(R_+) = -L_+m_\varphi(R_+)I_\varphi. \quad (8)$$

The concept of an effective layer air mass factor we introduced for scattered radiation is similar to the concept of an air mass factor introduced for direct radiation. According to Bouguer's law, the attenuation of sunlight by the atmosphere in the plane-parallel approximation is described by the expression

$$I^p = I_o^p\exp\left(-m\sum_i s_i\int c_i(h)dh\right),$$

where I^p is the intensity of radiation transmitted through the atmosphere, I_o^p is the radiation intensity at the top of the atmosphere, s_i is the absorption cross section of a gas with a concentration $c_i(h)$, and $m = 1/\cos z$ is the so-called air mass of the atmosphere for a solar zenith angle z. The coefficient m is equal to the ratio of the atmospheric optical thickness for a beam of light traveling at angle z to the optical thickness of the atmosphere for a perpendicularly incident beam. The intensity I_+^p in a perturbed atmosphere with gas concentration $c_i(h) + \Delta c_i(h)$ is

$$I_+^p = I^p\exp\left(-m\sum_i s_i\int\Delta c_i(h)dh\right). \quad (9)$$

Similarly, for direct radiation in a spherical atmosphere, we obtain

$$I_+^s = I^s\exp\left(-\int m(h)\sum_i s_i\Delta c_i(h)dh\right), \quad (10)$$

where $m(h) = 1/\cos z(h)$ and $z(h)$ is the angle at which the light crosses the layer. The coefficient $m(h)$ for a layer at height h has the same meaning as m for the entire atmosphere in (9).

The concept of a layer air mass factor is introduced for a spherical shell atmosphere. This approximation is used only for considerations of an analogy between air mass factors for direct and scattered radiation but is not extended to (5) and (6), which were obtained for calcu-

lating weighting functions. For a perturbation in a single layer, we find from (4) and (8) that

$$I_{+\varphi} = I_\varphi + w_\varphi(R_+)\Delta\sigma + o(\Delta\sigma)$$

$$= I_\varphi(1 - L_+ m_\varphi(R_+)\Delta\sigma) + o(\Delta\sigma)$$

$$= I_\varphi \exp(-L_+ m_\varphi(R_+)\Delta\sigma) + o(\Delta\sigma).$$

Accordingly, for a perturbation in the entire atmosphere, we have

$$I_+ = I\exp\left(-\int m(h)\sum_i s_i \Delta c_i(h)dh\right) + o(\|\Delta c\|). \quad (11)$$

Up to the small term $o(\|\Delta c\|)$, representation (11) is equivalent to equality (10), which relates direct sunlight (attenuated by the atmosphere) in the perturbed and unperturbed atmospheres. By analogy with direct sunlight, it is reasonable to call $m(h)$ the effective air mass factor of an atmospheric layer lying at height h for the given type of observations and the optical atmospheric conditions. The layer air mass factor shows how many times the light path is effectively increased (as compared with the geometric layer thickness) due to an inclined and repeated passage of the layer. Like the air mass factor for direct radiation, the effective layer air mass factor for scattered radiation is the same for all gases at a chosen wavelength. However, in contrast to the layer air mass factor for direct radiation, which is entirely determined by the angle $z(h)$ of light passage through the layer, the effective layer air mass factor depends not only on the observation direction and the sun's position but also on all optical characteristics of the atmosphere and the underlying surface.

In the foreign literature, the single scattering treatment makes use of concepts similar to layer air mass factors, namely, the enhancement factor of a layer [22, 23, 40] and the vertical shape factor [41].

FEATURES OF THE SOFTWARE CODE OF THE MODEL

The radiative transfer model described here calculates the intensity of scattered sunlight coming from a given direction in a spherical shell atmosphere. Multiple scattering is calculated by two Monte Carlo simulation techniques: by the method of conjugate random walks and by modified double local estimation [29]. The double local estimation requires less CPU time at twilight, when the sun is more than 3°–5° below the horizon. Single scattering can be calculated by the Monte Carlo techniques or by a faster direct integration method. The Monte Carlo method for multiple scattering used in combination with direct integration for single scattering requires the least CPU time. The choice of a spherical shell atmosphere is also explained by the desire to reduce CPU time (as compared with that required for a spherical asymmetric atmosphere).

The atmosphere in the model consists of spherical layers, each of which has constant optical characteristics. The intensity is computed simultaneously with the set of its derivatives with respect to the absorption cross section in all spherical layers. This algorithm is a modification of (7) and (8) for the implemented Monte Carlo simulation techniques. It is important that the time required for the simultaneous computation of intensities and all of their derivatives is only 1.2–1.8 times greater than the time required for computing intensities alone (for the same number of photon paths). The model also calculates the errors (variances) of estimated intensities and their derivatives.

The radiative transfer model takes into account gas absorption, aerosol scattering and absorption, Rayleigh scattering, and surface albedo. There is an option to switch to optical atmospheric characteristics linearly varying inside the layers (instead of the constant characteristics inside the layers used by default). The computations can be carried out with or without allowance for polarization. The use of C++ made it possible to implement various modifications of the code in the form of templates and allowed wide application of software reuse.

COMPARISONS OF MODELS

The radiative transfer model has participated in several international comparisons designed for viewing geometries for which the sphericity of the atmosphere plays an important role.

Simulation of ground-based twilight observations. Zenith sky radiances at the Earth's surface calculated by various models were compared in [42]. In addition to this author's model, spherical models without allowance for polarization took part in the comparison: a model with successive orders of scattering [43] and CDIPI [33]. The computations were carried out for solar zenith angles varying from 20° to 96° at the wavelengths 311, 332, 450, and 800 nm for a purely Rayleigh atmosphere and an atmosphere with aerosol. For solar zenith angles ranging from 20° to 93°, the differences between the models did not generally exceed 3%. For angles z larger than 94°, agreement better than 5% was achieved in comparison with the CDIPI model. The results published in [44] were used for an indirect comparison with GSS [45] and Dave's model [46], which take into account polarization. In the cases available for comparison (for solar zenith angles varying from 20° to 90° and for UV wavelengths), the differences between

the two models and this author's model with polarization did not exceed 1%.

Simulation of limb scattered radiance. The limb scattered radiances calculated by six models were compared in [47]. These were the aforementioned CDIPI [33] and GSS [45] models, this author's model, the SIRO spherical Monte Carlo model [48], and the LIMBTRAN [49] and CDI [33] pseudospherical models. The computations were carried out for the wavelengths 325, 345, and 600 nm and tangent heights of 10 to 60 km with a step of 5 km. The limb scattered radiances were computed for ray perigee solar zenith and azimuthal angles equal to 39.29° and 111.74°, respectively. This viewing geometry corresponds to the SOLSE/LORE experiment, in which limb scattered radiances were measured from the Space Shuttle in December 1997 [50]. The computations were conducted for a purely Rayleigh atmosphere and an atmosphere with aerosol, and the surface albedo was equal to 0 and 0.95. The computations were conducted with and without allowance for polarization. The results for the spherical models agreed within 3%. The differences of the approximate pseudospherical models (CDI and LIMBTRAN) from the spherical ones reached 5% and 8% for albedo of 0 and 0.95, respectively, and had a maximum at 60 km.

High-accuracy comparison. To understand the remaining discrepancies in computations [47], a finer comparison has been made between this author's model and the SIRO Monte Carlo model for the same limb-viewing geometry [51]. In the comparison reported in [47], the characteristics of the atmosphere were specified on a grid extending from 0 to 100 km with a step of 1 km, and the total absorption and scattering of the atmosphere were adjusted in each one-kilometer layer. The distribution function inside each layer was not prescribed. The SIRO model usually uses a linear distribution function, with continuity conditions imposed at the grid points. This author's model has a constant distribution function inside each layer. For a new comparison, the distribution functions inside the layers were adjusted more accurately. For this purpose, 0.2-km thick sublayers approximating the linear distribution of the SIRO model were introduced into this author's model, and additional layers ensuring a jump in the optical characteristics on the boundary of the one-kilometer layers were introduced into the SIRO model. As a result, the discrepancies between the models with adjusted distribution functions inside each layer were found to be less than 0.05–0.3% for both distribution functions. These values lie within the statistical error of the Monte Carlo computations executed. The differences between the radiances computed for two different distribution functions were the same for both models and varied monotonically from 0% at 10 km to 1% at 60 km. The radiances for a uniform distribution inside a layer were systematically lower than the radiances for a linear distribution function. In the other models compared in [47], the derivatives and integrals were computed by grid methods. Therefore, the function values between the grid points were not defined in those models. Probably, this could explain the several-percent discrepancies between their results. However, additional investigation (e.g., with a varying grid step) similar to that performed for the Monte Carlo models is required for verifying this explanation.

Comparison of computed layer air mass factors. For the same limb-viewing geometry as in [47], the layer air mass factors were computed [52] by this author's model and the CDI pseudospherical model [33]. The effective air mass factors were computed for one-kilometer atmospheric layers. Based on the comparison results, we can distinguish three basic regions of the atmosphere where the features of the algorithms for computing layer air mass factors and their accuracy manifest themselves differently.

(1) The first region is located two layers above the tangent height. The differences between the results of the two models in this region did not exceed 1%. The air mass factors of the layers take large values (as a rule, they range from 40 to 8, decreasing with height). A major contribution to the air mass factors is made by single scattering.

(2) The second region is located below the tangent height. The air mass factor of a layer in this region is entirely determined by multiple scattering. Typically, the air mass factors amount to 1.8–2.2. In the visible range, they increase up to 3.8 in the troposphere. Although the absolute differences between the air mass factors for the two methods remain small, the relative differences at heights of 50–60 km reach 30%. These differences are likely caused by the discrepancy in the multiple scattering calculations performed in the spherical and pseudospherical models; this discrepancy is known to increase with height. However, it should be noted that the accuracy of atmospheric retrievals should be much less affected by these differences because of the small air mass factors in the second region.

(3) The third region consists of two layers located above the tangent height h_0. In the absence of strong absorption in the overlying layers, the air mass factor quickly changes with height h, roughly as $1/sqrt(h - h_0)$. Therefore, the air mass factors in this region depend strongly on the computational algorithm and its actual vertical resolution. In this region, special attention should be given to the agreement between the resolutions of the algorithm and the measuring instrument. The typical values of air mass factors are 60–80. The differences between the air mass factors computed by the two methods are less than 1.5%.

Table

Model	CPU time	Computer
Spherical model, Rayleigh atmosphere		
January 2001 version without polarization	3*–17** s	PC Intel Pentium II 450 MHz
January 2001 version with polarization	13*–23** s	PC Intel Pentium II 450 MHz
Spherical model, atmosphere with aerosol		
March 2002 version without polarization	5*–6** s	PC AMD Athlon 1410 MHz
Simultaneous computation of intensities and effective air mass factors for 100 layers, spherical model, atmosphere with aerosol		
March 2002 version with polarization	6*–10** s	PC AMD Athlon 1410 MHz
Pseudospherical models, Rayleigh atmosphere without polarization		
CDI	5 s	PC AMD Athlon 750 MHz
LIMBTRAN	5–10 s	SGI 0200 4X, MIPS R10000

Notes: The table presents the CPU times required for computing the limb scattered radiances for a single wavelength and all tangent heights from 10 to 60 km with a step of 5 km. For the present model, the CPU time in all cases corresponds to radiances computed with 1% accuracy. The accuracy of the computed layer air mass factors is 0.8–4.2%. For comparison, the table lists the data for pseudospherical models from [47]. * for 600 nm, ** for 325 and 345 nm.

Comparison of CPU times. The CPU times required for computing limb scattered radiances were estimated in the framework of the comparisons in limb-viewing geometry in [47]. For the present model, the CPU time required for computing radiance with 1% accuracy was found to be 3–17 s. These values are comparable with CPU times for the CDI and LIMBTRAN pseudospherical models (5–10 s). The CPU time for the other fully spherical models (SIRO, GSS, and CDIPI) was 10–15 min [47]. More detailed information on CPU times for the present model is given in the table.

SOME APPLICATIONS

Let us analyze the influence exerted by the multiple scattering treatment on the accuracy of the trace gas contents determined from ground-based observations. The O_3 and SO_2 contents are determined from zenith sky radiances measured by Brewer and Dobson spectrophotometers in the UV spectral region [1, 11], and the contents of NO_2, O_3, and other gases are determined from NDSC zenith sky measurements in the visible spectral range [21–23, 53]. In the visible range, measurements are performed at twilight up to the solar zenith angle $z = 96°$, when the height of the Earth's shadow is as high as 50 km, which makes it possible to estimate the vertical distributions of gases below this boundary. In the Umkehr ozone retrieval method, measurements are performed for zenith angles of 60°–90°, but the movement of the UV shadow from the ozone layer makes it possible to retrieve vertical gas distributions at approximately the same heights.

The standard algorithm for ozone profile retrieval from Umkehr measurements is based on an approximate multiple scattering scheme [10], which can be described as follows. The dependence of the measured radiation on the ozone profile is linearized about the point corresponding to the average ozone profile magnitude. The radiation intensity is calculated at the linearization point with allowance for multiple scattering. However, the derivatives (weighting functions) with respect to the ozone profile, which is a vector parameter, are evaluated in the single scattering approximation. The simplified multiple scattering scheme leads to increased errors in ozone profile retrievals, which was first noted in [54]. This approach to the design of a retrieval algorithm is associated with the fact that the simplest and most frequently used method for calculating weighting functions involves the computation of intensities for an a priori ozone profile and a set of perturbed ozone profiles. Therefore, the CPU time required for computing exact weighting functions is proportional to the number of atmospheric layers (in which the intensities must be computed for perturbation) and becomes unacceptably long. As was mentioned above, the computational algorithm used in the model under consideration exhibits a qualitatively better CPU time.

Figures 1 and 2 show examples of air mass factors and weighting functions computed from Brewer spec-

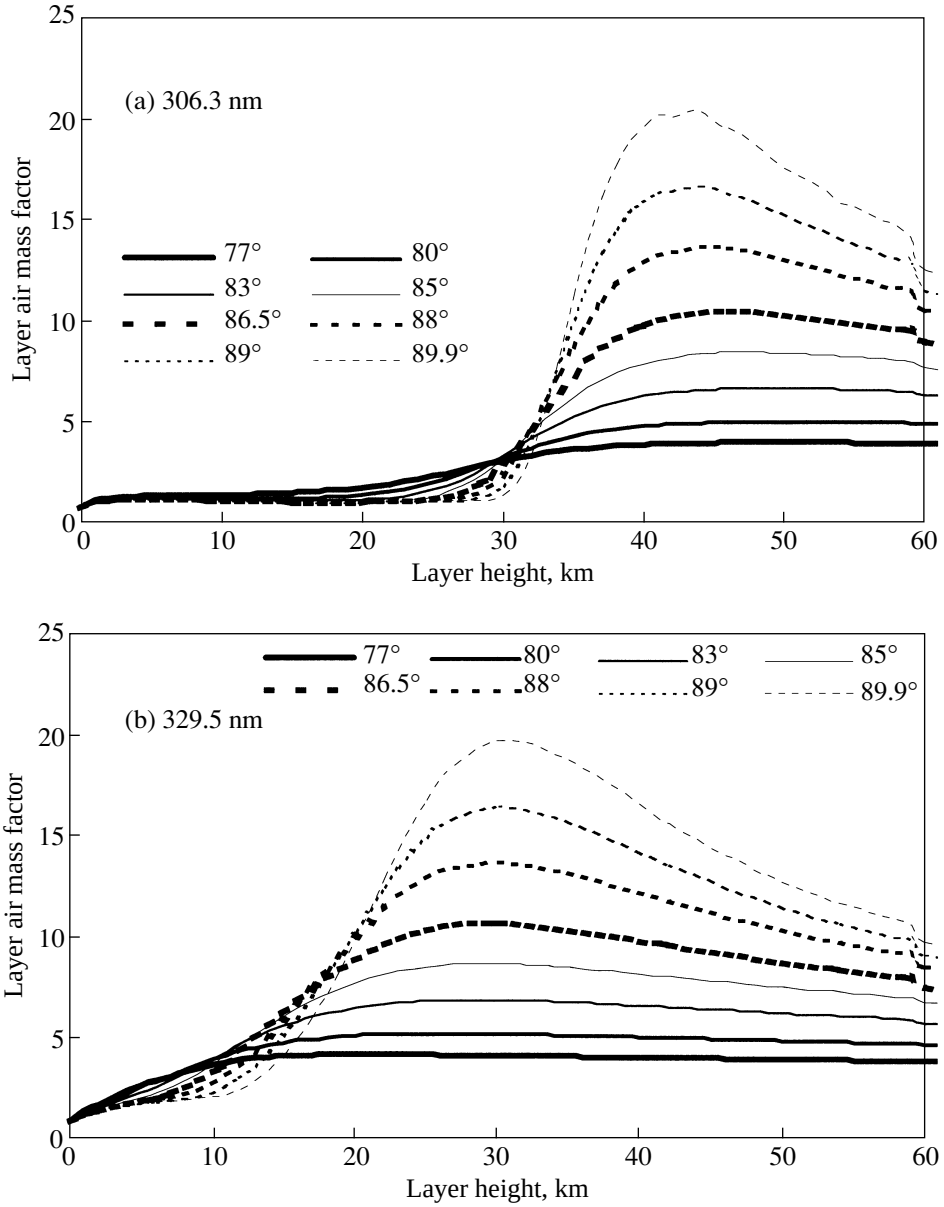

Fig. 1. Layer air mass factors of Umkehr ozone profile measurements for the solar zenith angles 77°, 80°, 83°, 85°, 86.5°, 88°, 89°, and 89.9° and the wavelengths (a) 306.3 nm and (b) 329.5 nm.

trophotometer measurements by the extended and standard Umkehr algorithms. In the standard Umkehr algorithm [10, 11], measured intensities are preliminarily transformed and their ratios at pairs of wavelengths are used for retrieval. The extended Umkehr algorithm proposed in [24] retrieves ozone profiles directly from intensities, which ensures its better accuracy (see curves *1* and *3* in Fig. 5). Figures 3 and 4 show the ratios of the approximate weighting functions calculated for single scattering to the exact weighting functions.

In the framework of the model used in [24], the accuracy of the algorithm based on approximate weighting functions was numerically compared with the accuracy of the algorithm based on weighting functions that take into account all orders of scattering. In both cases, the intensities were computed for all orders of scattering. The use of approximate weighting functions leads to increased retrieval errors not only below 15–20 km, where multiple scattering is important, but also at the other heights (see curves *2* and *4* in Fig. 5). The extended Umkehr algorithm is more sensitive to

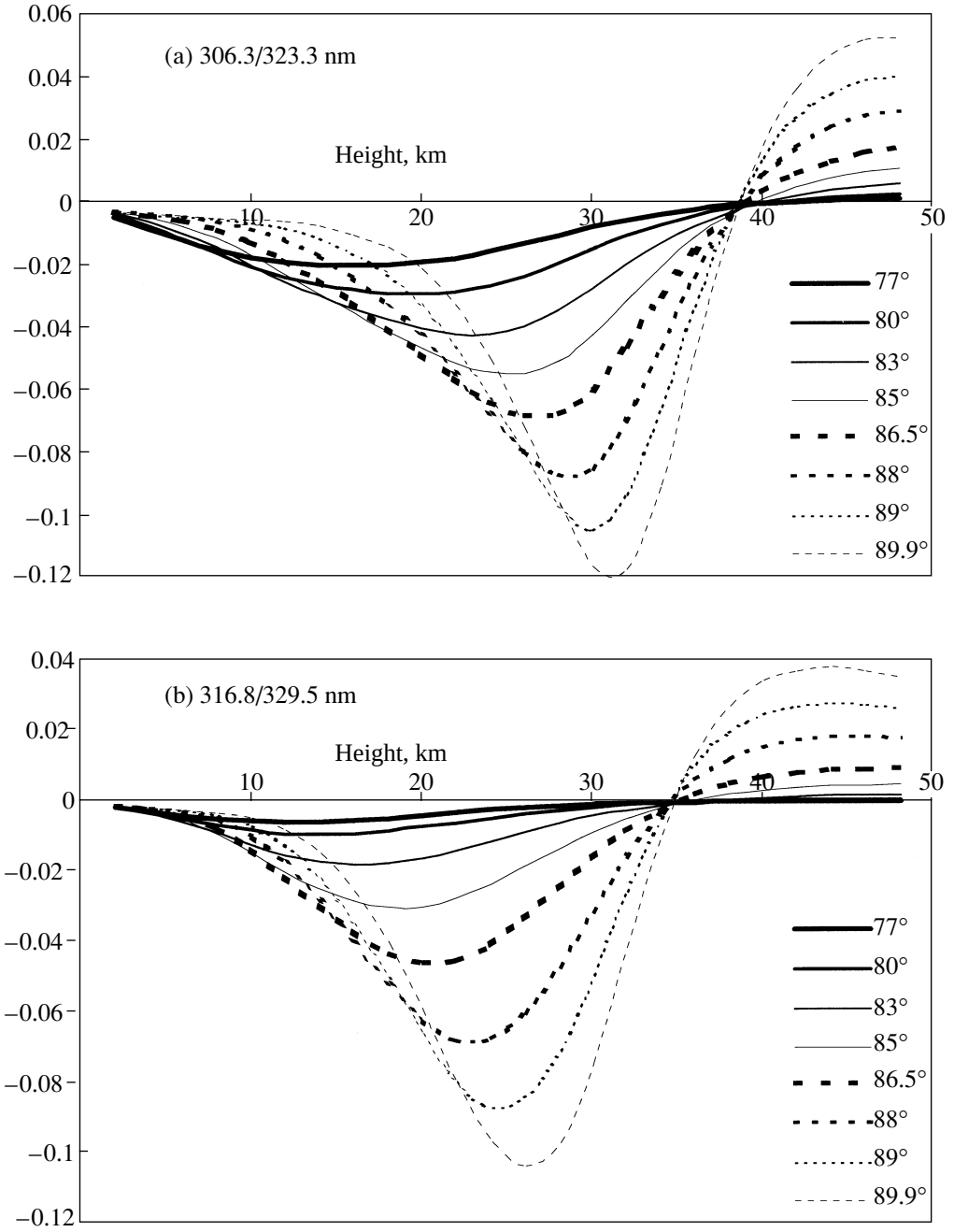

Fig. 2. Weighting functions for Umkehr ozone profile measurements after the intensities have been transformed into their ratios at pairs of wavelengths in the standard Umkehr algorithm. The pairs of wavelengths are (a) 306.3 and 323.3 nm and (b) 316.8 and 329.5 nm.

errors in radiative transfer computations than the standard algorithm. For exact weighting functions, the errors in the standard method are approximately twice as large as those in the extended method below 20 km, while for approximate weighting functions, this difference is about 10–20%.

The time required for computing intensities and all weighting functions in the Umkehr method, with the accuracy of the computed intensities being better than 1%, is 18.7 min on a PC AMD Athlon XP 1600+ (1410 MHz) with OS MS Windows 98SE (20.5 min on a PC Intel Pentium 4 1700MHz with OS MS Windows 2000) with the use of the Borland C++ 5.02 compiler. The computations are performed simultaneously for the wavelengths 306.3, 320.0, 310.0, 323.3, 313.5, 326.5, 316.8, and 329.5 nm at the solar zenith angles $z = 77°$,

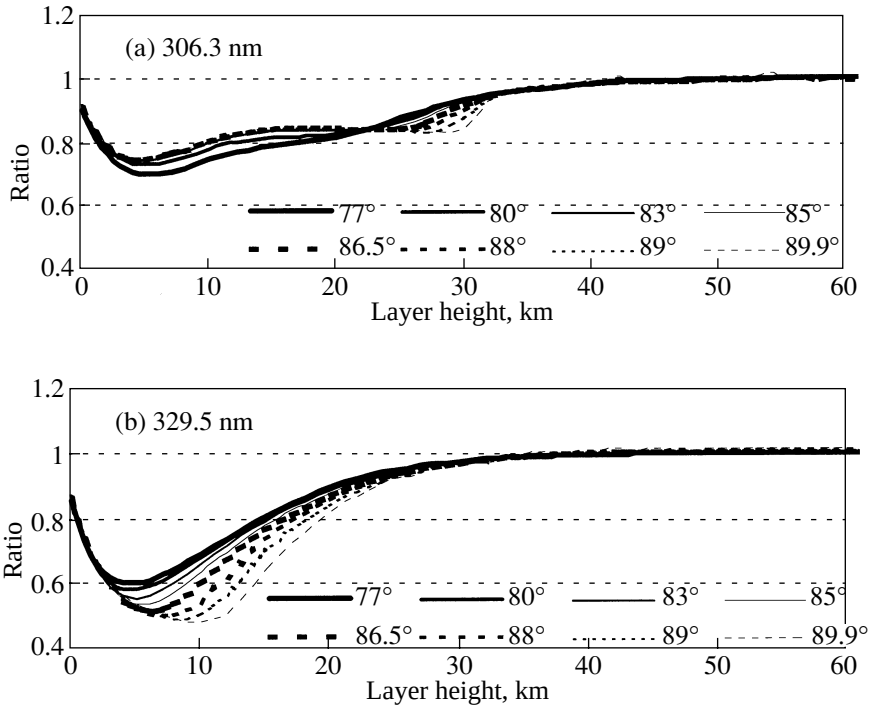

Fig. 3. Ratios of the Umkehr weighting functions calculated for single scattering to the exact weighting functions for the wavelengths (a) 306.3 nm and (b) 329.5 nm.

80°, 83°, 85°, 86.5°, 88°, 89°, and 89.9° and require the simulation of approximately 1.3 million paths of photons. The computed intensities have the best accuracy (0.1%) at the wavelength 329.5 nm and $z = 77°$ and have the worst accuracy (1%) at 306.3 nm and $z = 89.9°$. The accuracy of computed weighting functions for this number of photons is 0.12–1.5%. Because of these low CPU times, the multiple scattering can be computed with the use of all available data on the atmospheric optical conditions for every particular Umkehr measurement.

Vertical NO_2 profiles are retrieved from zenith sky observations near 450 nm. As in the case of Umkehr measurements, the NO_2 retrieval algorithms use weighting functions calculated in the single scattering approximation. The first steps in the multiple scattering calculation of weighting functions were taken in [55]. Figure 6 shows the layer air mass factors computed with allowance for all orders of scattering, and Fig. 7 displays their ratios to the air mass factors computed in the single scattering approximation. The approximate layer air mass factors underestimate the exact ones below 20 km and overestimate them above 30 km for all used solar zenith angles z varying from 84° to 96°. For all zenith angles, the difference has a maximum between 5 and 10 km. The difference in this region reaches –30% at $z = 84°$ and –70% at $z = 96°$. Between 20 and 30 km, the approximate air mass factors comprise more than 95% of the exact air mass factors for zenith angles lower than 93°. However, the difference increases up to –25% for $z = 96°$. Above 30 km, the approximate computations differ negligibly from the exact ones up to $z = 93°$, but the difference increases to +20% for $z = 96°$.

Based on the comparison results for layer air mass factors, we can conjecture the influence exerted by single scattering computations on the accuracy of NO_2 retrievals. Since different ranges of solar zenith angles are used to retrieve total NO_2 contents and NO_2 profiles, the character of influence may be different. Zenith angles less than 94° are used for total NO_2 retrievals, and the maximum NO_2 content corresponds to the zone where the approximate computations have the best accuracy. Therefore, it should be expected that the reduction in the accuracy caused by using approximate air mass factors is limited to several percent. An exception may be observations at an increased NO_2 content in the troposphere, when the use of approximately computed air mass factors can substantially degrade the retrievals because of the large errors below 15 km. Zenith angles smaller than $z = 96°$ are used for NO_2 profile retrievals. The large errors in the air mass factors computed in the single scattering approximation for zenith angles 94°–96° virtually in the entire range of

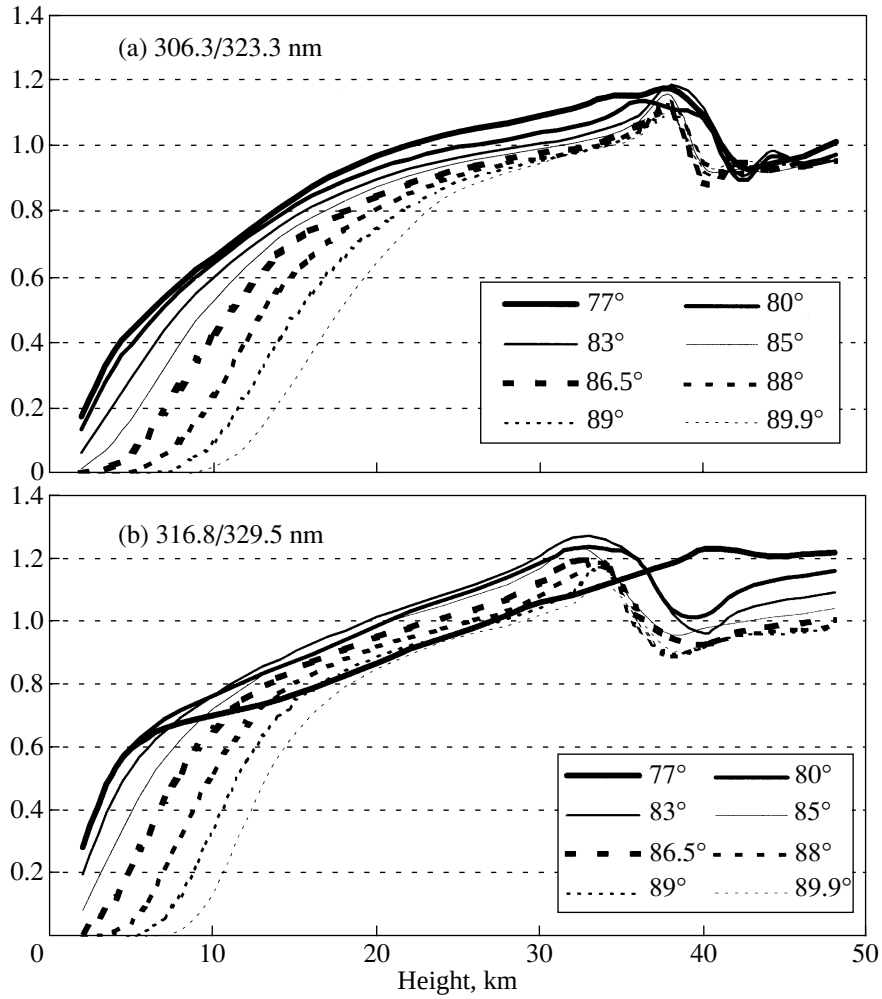

Fig. 4. Ratios of the weighting functions calculated for single scattering to the exact weighting functions for the standard Umkehr method. The pairs of wavelengths are (a) 306.3 and 323.3 nm and (b) 316.8 and 329.5 nm.

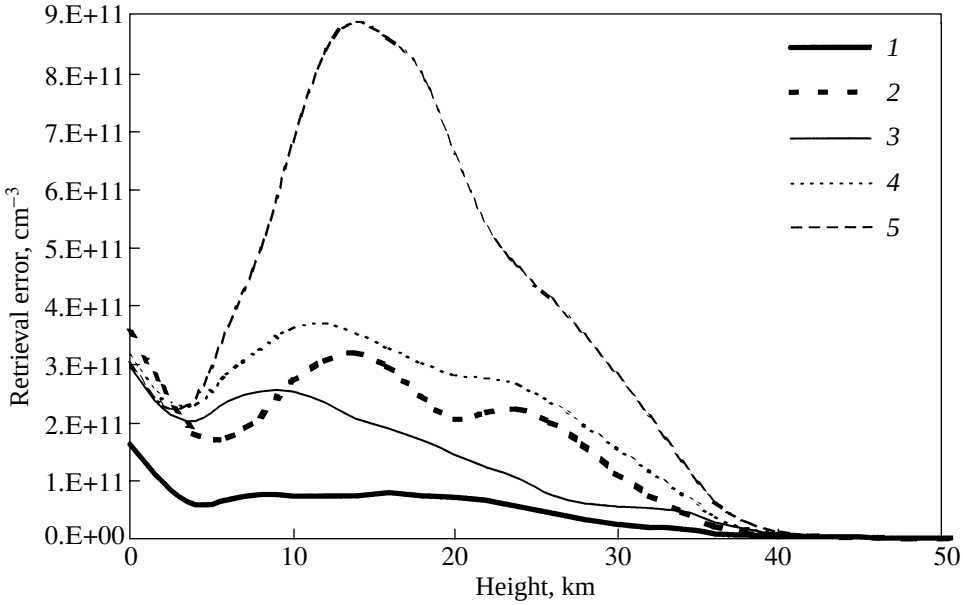

Fig. 5. Rms error in the ozone profile retrieval (curves *1–4*) and its rms climatic variations (*5*). Curves *1* and *3* correspond to the extended and standard Umkehr methods, respectively, based on exact weighting functions; and curves *2* and *4* correspond to the extended and standard Umkehr methods, respectively, based on approximate weighting functions.

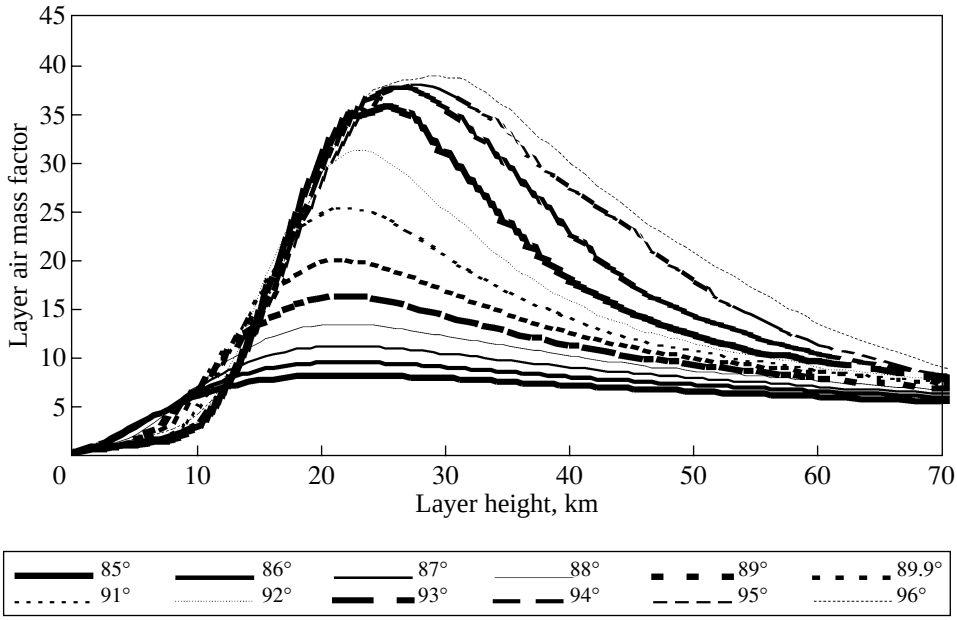

Fig. 6. Layer air mass factors of twilight nitrogen dioxide measurements for the solar zenith angles 84°–96° and the wavelength 450 nm.

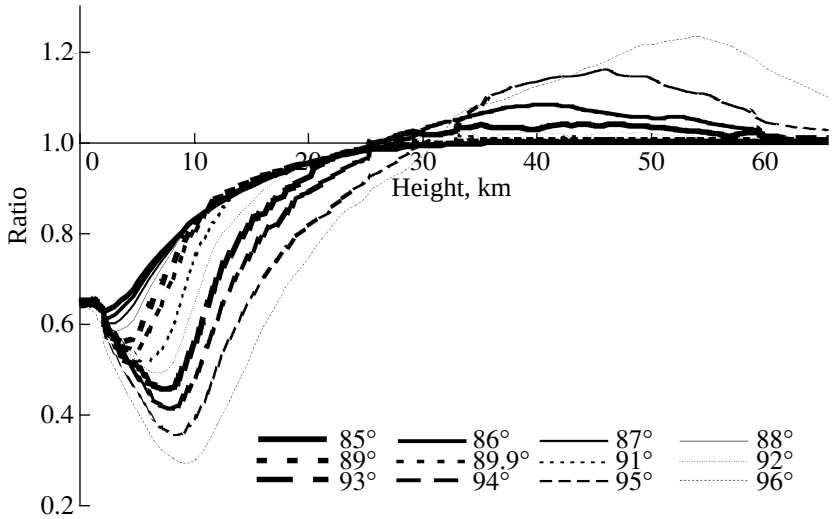

Fig. 7. Ratios of the approximate (single scattering) to exact layer air mass factors of twilight nitrogen dioxide measurements for the wavelength 450 nm.

heights can likely lead to systematic errors in NO_2 profile retrievals up to several tens of percent even above 30 km.

CONCLUSIONS

A spherical radiative transfer model has been designed for using in inverse problems of atmospheric optics. The model calculates intensities and their derivatives with respect to absorption. In other notations, these derivatives are known as weighting functions or layer air mass factors. Multiple scattering radiation in the model is evaluated by Monte Carlo simulation techniques: by the method of conjugate random walks or by modified double local estimation. The model can be run with or without allowance for polarization, Rayleigh and aerosol scattering, gas and aerosol absorption, and Lambert surface albedo. A spherical shell atmosphere is used to reduce the CPU time required for running the model.

The speed of intensity computations accurate to 1% is approximately the same as in the other authors' pseudospherical models used for comparison. The time

required for simultaneous computation of intensities and their derivatives is only 1.2–1.8 times as much as the time required for the computation of intensities alone.

The model was compared with other spherical and pseudospherical models for geometries in which the sphericity of the atmosphere is important: twilight observations from the ground and limb scattered observations from space. The layer air mass factors calculated by different models were also compared. For complete and accurate agreement between the vertical profiles of atmospheric optical characteristics, the model results were found to agree with the SIRO Monte Carlo model [48] within 0.1–0.3%, which corresponds to the statistical errors of the computations. When the optical characteristics of the models compared were adjusted on a grid with a step of 1 km, the agreement with ground-based observations was better than 3% for solar zenith angles z smaller than 93° and was better than 5% for angles z in the range 94°–96°; for limb scattered observations, the agreement between the spherical models was better than 3%.

The additional ozone retrieval errors resulting from the single scattering approximation used for computing weighting functions were estimated for the Umkehr method used as an example. The layer air mass factors for twilight measurements of nitrogen dioxide were computed with allowance for multiple scattering radiation. The character of the influence exerted on nitrogen dioxide retrievals by the air mass factors computed in the single scattering approximation was conjectured based on a comparison of approximate and exact air mass factors. The CPU time required for computing weighting functions with allowance for all orders of scattering suggests that the radiative transfer model developed can be directly used in retrieval algorithms.

ACKNOWLEDGMENTS

I am grateful to S.A. Ukhinov for our meeting 12 years ago, which was very useful for this work. I am grateful to Liisa Oikarinen and Alexej Rozanov for their fast response and support of the initiatives to expand model comparison. I am grieving at the tragic death of L. Oikarinen.

This work was supported by the Russian Foundation for Basic Research, project no. 01-05-64546.

REFERENCES

1. G. M. B. Dobson, Forty Years' Research on Atmospheric Ozone at Oxford: A History, Appl. Opt. **7**, 401 (1968).
2. A. W. Brewer, C. T. McElroy, and Kerr, J. B., Nitrogen Dioxide Concentrations in the Atmosphere, Nature (London) **246** (5429), 129–133 (1973).
3. J. F. Noxon, Nitrogen Dioxide in the Stratosphere and Troposphere Measured by Ground Based Absorption Spectroscopy, Science **189**, 547–549 (1975).
4. D. Perner and U. Platt, Detection of Nitrous Acid in the Atmosphere by Differential Optical Absorption, Geophys. Res. Lett. **7**, 1053–1056 (1979).
5. G. I. Kuznetsov, "Multiwave Method and Instrumentation for Studies Atmospheric Ozone and Aerosol," Izv. Akad. Nauk SSSR, Fiz. Atmos. Okeana **11**, 647–651 (1975).
6. N. F. Elanskii, A. Ya. Arabov, A. S. Elokhov, *et al.*, "Observations of Minor Atmospheric Gases and UV Radiation at the Kislovodsk High-Altitude Scientific Station," Izv. Akad. Nauk, Fiz. Atmos. Okeana **31**, 10–19 (1995).
7. V. N. Aref'ev, N. E. Kamenogradskii, V. K. Semenov, and V. P. Sinyakov, Ozone and Nitrogen Dioxide in the Atmosphere over Northern Tian Shan, Izv. Akad. Nauk, Fiz. Atmos. Okeana **31**, 20–25 (1995).
8. M. P. McCormick, SAGE II: An Overview, Adv. Space Res. **7** (3), 219–226 (1987).
9. I. N. Ivanova, A. F. Chizhov, G.A. Kokin, *et al.*, Some Results of Polar Ozonosphere Investigation by Optical Ground, Rocket and Satellite Methods, in *Proceedings of 19th Annual European Meeting on Atmospheric Studies by Optical Methods* (Sweden, Kiruna, 1992), pp. 29–41.
10. C. L. Mateer and J. J. Deluisi, A New Umkehr Inversion Algorithm, J. Atmos. Terr. Phys. **54**, 537–556 (1992).
11. C. T. McElroy and J. B. Kerr, Table Mountain Ozone Intercomparison: Brewer Ozone Spectrophotometer Umkehr Observations, J. Geophys. Res. **100**, 9293–9300 (1995).
12. D. F. Heath, A. J. Krueger, H. A. Roeder, and B. D. Henderson, The Solar Backscatter and Total Ozone Mapping Spectrometer (SBUV/TOMS) for Nimbus 7, Opt. Eng. **14**, 323–313 (1975).
13. O. A. Volkovitskii, A. V. Kal'sin, T. V. Kozina, *et al.*, "Measurements of the Total Content of Ozone and Its Vertical Distribution from the Meteor-3 Spacecraft," Izv. Akad. Nauk, Fiz. Atmos. Okeana **29**, 646–652 (1993).
14. A. V. Poberovskii, A. V. Polyakov, Yu. M. Timofeev, *et al.*, "Ozone Profile Determination by Occultation Sounding from the "Mir" Space Station: 1. Instrumentation and Data Processing Method," Izv. Akad. Nauk, Fiz. Atmos. Okeana **35** (3), 312–321 (1999) [Izv., Atmos. Ocean. Phys. **35** (3), 282–290 (1999)].
15. J. P. Burrows, M. Weber, M. Buchwitz, *et al.*, The Global Ozone Monitoring Experiment (GOME): Mission Concept and First Scientific Results, J. Atmos. Sci. **56**, 151–175 (1999).
16. E. J. Llewellyn *et al.*, OSIRIS—An Application of Tomography for Absorbed Emissions in Remote Sensing, in *Applications of Photonic Technology 2*, Ed. by G. A. Lampropoulos and R. A. Lessard (Plenum, New York, 1997), pp. 627–632.
17. M. P. McCormick, J. M. Zawodny, W. P. Chu, *et al.*, Stratospheric Aerosol and Gas Experiment III (SAGE III), *SPIE Int. Symp. for Opt. Eng.* (Orlando, 1993).
18. H. Bovensmann, J. P. Burrows, M. Buchwitz, *et al.*, SCIAMACHY: Mission Objectives and Measurement Modes, J. Atmos. Sci. **56**, 127–150 (1999).

19. J. L. Bertaux, G. Megie, T. Widemann, *et al.*, Monitoring of Ozone Trend by Stellar Occultations: The GOMOS Instrument, Adv. Space Res. **11**, 237–242 (1991).
20. J. Larsen *et al.*, Algorithm Theoretical Basis Document (Limb Profile Ozone) for the Ozone Mapped and Profile Suit (OMPS) of the NPOESS Satellite System, Document No. IN0092A-107 (Ball Aerospace System Division, Boulder, 1999).
21. J. F. Noxon, E. C. Whipple, and R. S. Hyde, Stratospheric NO^2. 1. Observation Method and Behaviour at Midlatitudes, J. Geopys. Res. **84**, 5047–5076 (1979).
22. S. Solomon, A. L. Schmeltekopf, and R. W. Sanders, On the Interpretation of Zenith Sky Absorption Measurements, J. Geophys. Res. **92** (7), 8311–8319 (1987).
23. R. L. McKenzie, P. V. Johnston, C. T. McElroy, *et al.*, Altitude Distributions of Stratospheric Constituents from Ground-Based Measurements at Twilight, J. Geophys. Res. **96**, 15 499–15 511 (1991).
24. N. F. Elansky, I. V. Mitin, and O. V. Postylyakov, "Maximum Accuracy of Umkehr Measurements of Vertical Ozone Profiles," Izv. Akad. Nauk, Fiz. Atmos. Okeana **35** (1), 73–85 (1999) [Izv., Atmos. Ocean. Phys. **35** (1), 65–77 (1999)].
25. O. V. Postylyakov, N. F. Elansky, A. S. Elokhov, *et al.*, Determination of Aerosol Vertical Profile Using Measurements of the Polarized Zenith-Sky Radiance during Twilight: Model, Retrieval Algorithm and First Measurements, in *Proceedings of Quadrennial Ozone Symposium* (Sapporo, 2000), pp. 595–596.
26. C. D. Rodgers, Characterization and Error Analyses of Profiles Retrieved from Remote Sensing Measurements, J. Geophys. Res. **95**, 5587–5595 (1990).
27. G. I. Marchuk, "Value Equation for Information from Meteorological Satellites and Inverse-Problem Statement," Kosm. Issled. **2**, 462–477 (1964).
28. G. A. Mikhailov, "Monte Carlo Calculation of Derivatives of Functionals of the Solution to the Transfer Equation with Respect to the System's Parameters," Zh. Vychisl. Mat. Mat. Fiz. **7**, 915–919 (1967).
29. G. I. Marchuk, G. A. Mikhailov, M. A. Nazaraliev, *et al.*, *Monte Carlo Method in Atmospheric Optics*, Ed. by G. I. Marchuk (Nauka, Novosibirsk, 1976) [in Russian].
30. V. V. Rozanov, D. Diebel, R. J. D. Spurr, and J. P. Burrows, GOMETRAN: A Radiative Transfer Model for the Satellite Project GOME, the Plane Parallel Version, J. Geophys. Res. **102**, 16683–16695 (1997).
31. R. J. Spurr, T. P. Kurosu, and K. V. Chance, A Linearised Discrete Ordinate Radiative Transfer Model for Atmospheric Remote Sensing Retrieval, J. Quant. Spectrosc. Radiat. Transfer **68**, 689–735 (2001).
32. J. Landgraf, O. P. Hasekamp, M. A. Box, and T. Trautmann, A Linearized Radiative Transfer Model for Ozone Profile Retrieval Using the Analytical Forward-Adjoint Perturbation Theory Approach, J. Geophys. Res. **106**, 27291–27305 (2001).
33. A. Rozanov, V. Rozanov, and J. P. Burrows, A Numerical Radiative Transfer Model for a Spherical Planetary Atmosphere: Combined Differential-Integral Approach Involving the Picard Iterative Approximation, J. Quant. Spectrosc. Radiat. Transfer **69**, 491–512 (2001).
34. E. A. Ustinov, "Inverse Problem of Photometric Observations of the Solar Radiation Reflected from an Optically Thick Atmosphere: A Mathematical Method and Weight Functions of a Linearized Inverse Problem," Kosm. Issled. **29**, 519–532 (1991).
35. E. A. Ustinov, Adjoint Sensitivity Analysis of Radiative Transfer Equation Temperature and Gas Mixing Ratio Weighting Functions for Remote Sensing Atmospheres in Thermal IR, J. Quant. Spectrosc. Radiat. Transfer **68**, 195–211 (2001).
36. M. Box and C. Sendra, Sensitivity of Existing Radiances to Details of Scattering Phase Function, J. Quant. Spectrosc. Radiat. Transfer **54**, 695–703 (1995).
37. M. N. Nazaraliev, *Statistical Modeling of Radiative Processes in the Atmosphere* (Nauka, Novosibirsk, 1990) [in Russian].
38. G. A. Mikhailov, *Monte Carlo Weight Methods* (SO Ross. Akad. Nauk, Novosibirsk, 2000) [in Russian].
39. V. S. Antyufeev, *Monte Carlo Method for Solving Inverse Problems of Radiation Transfer* (V.S.P. Int. Science, 2000).
40. L. M. Perlinski and S. Solomon, On the Evaluation of Air Mass Factors for Atmospheric Near-Ultraviolet and Visible Absorption Spectroscopy, J. Geophys. Res. **98**, 10363–10374 (1993).
41. P. I. Palmer *et al.*, Air Mass Factor Formulation for Spectroscopic Measurements from Satellites: Application to Formaldehyde Retrievals from the Global Ozone Monitoring Experiment, J. Geophys. Res. **106**, 14539–14550 (2002).
42. O. V. Postylyakov, Yu. E. Belikov, Sh. S. Nikolaishvili, and A. Rozanov, A Comparison of Radiation Transfer Algorithms for Modelling of the Zenith Sky Radiance Observations Used for Determination of Stratospheric Trace Gases and Aerosol, in *IRS 2000: Current Problems in Atmospheric Radiation*, Ed. by W. L. Smith and Yu. M. Timofeyev (Deepak, Hampton, 2001), pp. 885–888.
43. Yu. Belikov, Yu. Romanovsky, Sh. Nikolaishvili, and R. Peradze, Numerical Model of Scattering Radiation in the Earth Atmosphere for Scientific Investigations and Applications, J. Phys. Chem. Earth **25** (B), 427–430 (2000).
44. I. Petropavlovskih, J. DeLuisi, B. Herman, *et al.*, A Comparison of Radiance Calculations by Spherical Atmosphere Radiation Transfer Codes for Modeling the Umkehr Effect, in *Proceedings of XVIII Quadrennial Ozone Symposium*, Ed. by R. D. Bojkov and G. Visconti (1998), pp. 163–167.
45. B. M. Herman, A. Ben-David, and K. J. Thome, Numerical Techniques for Solving the Radiative Transfer Equation for a Spherical Shell Atmosphere, Appl. Opt. **33**, 1760–1770 (1994).
46. J. V. Dave, Effect of Aerosol Estimation of Total Ozone in an Atmospheric Column from the Measurements of Its Ultraviolet Radiance, J. Atmos. Sci. **26**, 716–726 (1978).
47. L. Oikarinen, E. Griffioen, R. Loughman, *et al.*, Comparison of Radiative Transfer Models for Limb-Viewing Scattered Sunlight Measurements, EOS Trans. AGU. 2001. **82** (47), Fall Meet. Suppl. Abstract A21B-0067.
48. L. Oikarinen, E. Sihvola, and E. Kyrölä, Multiple Scattering Radiance in Limb-Viewing Geometry, J. Geophys. Res. **104**, 31261–31274 (1999).

49. E. Griffioen and L. Oikarinen, LIMBTRAN: A Pseudo Three-Dimensional Radiative Transfer Model for the Limb-Viewing Imager OSIRIS on the Odin Satellite, J. Geophys. Res. **105**, 29717–29730 (2000).
50. R. D. McPeters, S. J. Janz, E. Hilsenrath, *et al.*, The Retrieval of O_3 Profiles from Limb Scatter Measurements: Results from the Shuttle Ozone Limb Sounding Experiment, Geophys. Res. Lett. **27**, 2597–2600 (2000).
51. O. V. Postylyakov, L. Oikarinen, and E. Kyrölä, Fine Comparison of Radiative Transfer Models for Scattering Limb Simulation, Geophys. Res. Abs. **5**, Abs. 05566 (2003).
52. O.V. Postylyakov and A. V. Rozanov, "Comparison of Layer Air Masses and the Weight Functions of an Inverse Problem Calculated from Radiative-Transfer Models Used to Interpret Ground-Based and Satellite Measurements," in *Tezisy Mezhd. simp. SNG "Atmosfernaya radiatsiya"* (MSAR-02), (St. Petersburg, 2002), pp. 30–31.
53. U. Platt, Differential Optical Absorption Spectroscopy (DOAS), in *Air Monitoring by Spectroscopic Techniques, Chem. Anal. Ser.* **127**, Ed. by M. W. Sigrist (Wiley, New York, 1997), pp. 27–84.
54. N. F. Elansky and O. V. Postylyakov, The Extended Brewer Umkehr Algorithm for Ozone Profile Retrieval: An Improved Approach to Multiple Scattering Consideration, in *Proceedings of Quadrennial Ozone Symposium* (Sapporo, 2000), pp. 359–360.
55. H. K. Roscoe *et al.*, Slant Column Measurements of O_3 And NO_2 during the NDSC Intercomparison of Zenith-Sky UV-Visible Spectrometers in June 1996, J. Atmos. Chem. **32**, 281–314 (1999).
56. O. V. Postylyakov and I. V. Mitin, "Analysis of the Accuracy of Retrieving the Vertical Distributions of Ozone and Nitrogen Dioxide from Ground-Based Observations with Allowance for Multiple Scattering in the Weight Functions of the Problem," in *Tezisy Mezhd. simp. SNG "Atmosfernaya radiatsiya" (MSAR-02)* (St. Petersburg, 2002), pp. 141–142.
57. S. A. Ukhinov and D. I. Yurkov, Computation of the Parametric Derivatives of Polarized Radiation and the Solution of Inverse Atmospheric Optics Problems, Russ. J. Numer. Anal. Math. Modelling **17**, 283–303 (2002).
58. O. V. Postylyakov, O. S. Ugolnikov, and I. A. Maslov, Effect of Aerosol and Multiple Scattering on Polarisation of Skylight during Twilight, Abstracts of European Aerosol Conference, J. Aerosol Sci. **2** (Suppl.), 1141–1142 (2003).

Translated by I. Ruzanova